

# Robust Controller Design for DFIG based Wind Conversion System using Direct Synthesis Approach

Sarfaraz Nawaz Syed<sup>a</sup>, Dr S.Tara Kalyani<sup>b</sup>

<sup>a</sup> Research Scholar, JNTUH & Associate Professor, Gokaraju Rangaraju Institute of Engineering and Technology, Hyderabad

<sup>b</sup> Professor & Controller of Examinations, JNTUH, Hyderabad

**Abstract:** The paper deals with the performance checking of an optimally designed PID controller with first order filter (PIDF) connected along the grid-side converter (GSC) in a doubly fed induction generator (DFIG) based wind energy conversion system (WECS). Initially, a relay test is conducted to scale back the upper order model of DFIG system to lower order model with dead time. The main objective of proposed controller to protect the system deterioration under various critical conditions such as external disturbances and parameters variation of DFIG. The PID controller parameters are obtained using the direct synthesis method. A systematic guideline is usually recommended for the choice of the tuning parameter of filter. Ultimately, system performance is tested and compared consistent with tracking, durability, distortion reduction. The method provides a significant improvement in the performance of the closed loop. Kharitonov theorem is used to check the robustness of the system. The simulation results indicate the effective use of proposed method into DFIG system in terms of tracking as well as unwanted distortion. The proposed approach goes further in the control of DFIG and wind energy conversion systems over the other existing methods.

**Keywords:** DFIG, PID controller, Direct Synthesis, Relay based identification, Interval polynomial

## Abbreviations:

DFIG = Doubly Fed Induction Generator

WECS = Wind Energy Conversion System

GSC = Grid Side Converter

RSC = Rotor Side Converter

VSC = Voltage Source Converter

VSWT = Variable Speed Wind Turbine

PCC = Point of Common Coupling

MIMO = Multiple Input Multiple Output

SISO = Single Input Single Output

PI = Proportional Integral

PID = Proportional Integral Derivative

PIDF = PID with First order filter

SOPDT = Second Order Plus Dead Time

ITAE = Integral Time-weighted Absolute Error

IAE = Integral Absolute Error

ISE = Integral Squared Error

TV = Total Variation

## 1. Introduction

Growing fuel prices and environmental problems such as air pollution are leading to various energy surveys. At the same time, there is an ongoing search for alternative distribution systems as existing power transmission systems are more expensive and naturally complex. Distributed generation i.e. direct use of renewable energy sources when loading is one possible option (Ravichandran S. et al. 2014- Kumar R. et al. 2019). This leads to the removal of transmission and distribution losses and the improvement of the reliability of the power supply. The power converter is used to connect renewable energy sources such as wind, solar, etc., and existing energy. A dual power inverter is a widely used power converter. But the use of those power converters leads to an undesirable harmonic generation that affects all loads near the common junction of the main grid (Mebrшту F. et al. 2020- Singh Bhim et al. 2010). Therefore, a filter is required for all such converters to minimize the effects of high-frequency pulse-wide modulation (PWM) below the desired limits (Huabin Wen et al. 2014).

Typically, a vector control strategy in the form of stator voltage controlled or may be stator flux oriented, is suggested to control DFIG. This approach shifts the DFIG system for nonlinear MIMO DFIG system into two single loop SISO systems representing direct currents and quadrature currents respectively (Taveiros F.E.V et al.

2015). A PI controller is employed in each loop in order to get the required apparent power control of DFIG system. In the literature it is given that system performance depends on the parameters of DFIG particularly rotor resistance to modify the vector control strategy (Pena R. et al. 1996). Therefore, closed loop control performance decreases when the DFIG parameters are changed due to temperature variations, magnetic saturations, etc.

In order to overcome this difficulty, a control methodology consisting of PIDF controller in the current control loop is suggested. Design of controller for higher order process is not convenient. So, in this paper, the higher order dynamics of DFIG is reduced to a SOPDT model using relay based identification technique (Åstrom K.J. & Hägglund T. 1984).

In general, an easy control structure with an easy controller is attractive because it is extremely easy for the operator to tune. In the current task, using direct synthesis approach to track desired output, a simple control method is developed with only one tuning parameter for all critical conditions of DFIG system.

In section II, DFIG configuration with operating principle is studied. Subsequently, modeling of DFIG is presented in section III. After that, the relay based identification is made in section IV. The design of PIDF controller is given in section V following the selection of tuning parameter in section VI. The performance measure is discussed in section VII. Simulation results and discussion are provided in Section VIII. The robustness analysis using Kharitonov theorem is described in section IX. Eventually, the paper ends with the conclusions.

## 2. DFIG Configuration with Operating Principle

A typical schematic circuit diagram of the DFIG based WECS with the proposed controller between GSC and PCC near the grid is exhibited in Figure. 1. Once the wind energy is converted into mechanical energy, it is then transformed into electrical energy which is directly supplied to the individual load or to the utility grid (Tremblay E. et al. 2011 - MaK. et al. 2015).

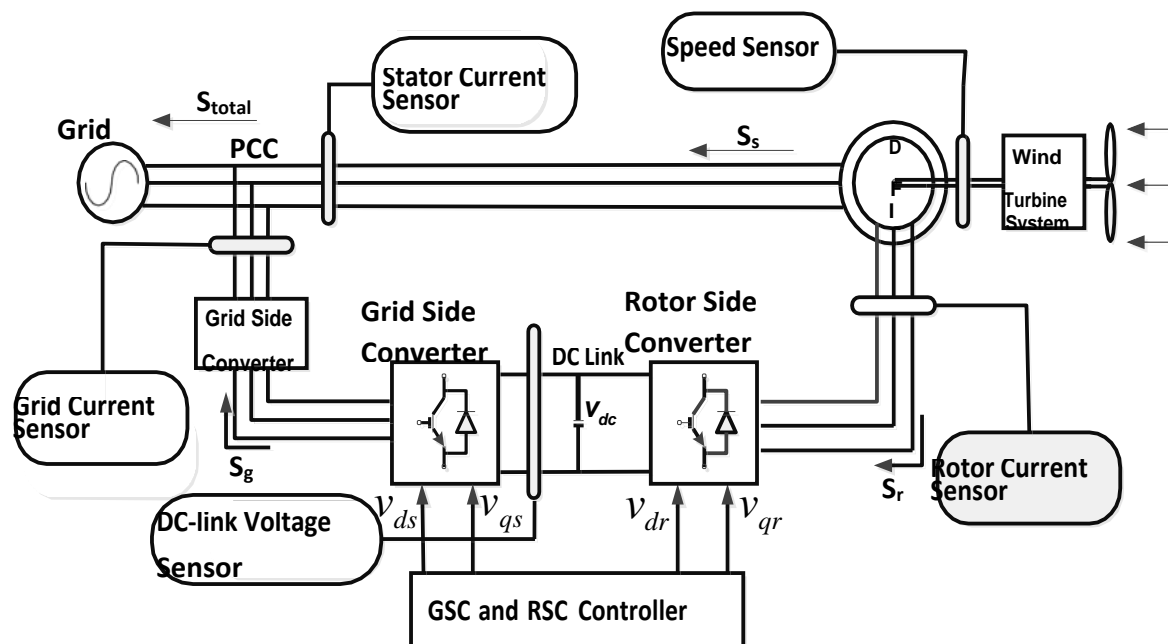


Figure.1 Schematic circuit diagram of DFIG based WECS

Here, a VSWT is linked to the DFIG shaft with a gear box. The stator and grid are coupled directly to each other and the rotor is connected to the grid via a back-to-back VSC (Swain S. & Ray P.K. 2017). These two converters use two different vector control schemes for synchronous reference frames. These converters use 30% of the total generator power (Swain S. & Ray P.K. 2017 - Mishra A. et al. 2018). A DC link connects RSC with the GSC creates a reversal scheme. The RSC controls the apparent power output at the grid terminals, while the GSC monitors the DC link voltage. GSC switching controls introduce harmonics where conventional coupling distorts PCC power.

### 3. Modeling of DFIG

Stator winding voltage expressions in d-q reference frame (**Bharti O. P. et al. 2016**) are

$$V_{qs} = R_s I_{qs} + \omega_s \psi_{ds} + \frac{d\psi_{qs}}{dt} \quad (1)$$

$$V_{ds} = R_s I_{ds} - \omega_s \psi_{qs} + \frac{d\psi_{ds}}{dt} \quad (2)$$

Where

$$\psi_{ds} = L_s I_{ds} + M I_{dr} \quad (3)$$

$$\psi_{qs} = L_s I_{qs} + M I_{qr} \quad (4)$$

Similarly, Rotor winding voltage expressions in d-q reference frame are

$$V_{qr} = R_r I_{qr} + (\omega_s - \omega) \psi_{dr} + \frac{d\psi_{qr}}{dt} \quad (5)$$

$$V_{dr} = R_r I_{dr} - (\omega_s - \omega) \psi_{qr} + \frac{d\psi_{dr}}{dt} \quad (6)$$

where

$$\psi_{dr} = M I_{ds} + L_r I_{dr} \quad (7)$$

$$\psi_{qr} = M I_{qs} + L_r I_{qr} \quad (8)$$

The real part of apparent power is

$$P_s = V_{ds} I_{ds} + V_{qs} I_{qs} \quad (9)$$

And the imaginary part is

$$Q_s = V_{qs} I_{ds} - V_{ds} I_{qs} \quad (10)$$

The developed torque  $T$  is obtained as

$$T = \frac{P_s M (I_{dr} \psi_{qs} - I_{qr} \psi_{ds})}{L_s} \quad (11)$$

So, to easily control the DFIG, it is possible to achieve independent control of the apparent power in the form of stator flux. The main objective is to align the stator flux in line with d axis (**Swami Naidu N. K. & Singh B. 2016**). Thus,

$$\psi_{ds} = \psi_s, \psi_{qs} = 0 \quad (12)$$

Neglecting stator resistance (**Kraus F. et al. 1992- Matušů R. & Prokop R. 2012**) and considering

$$V_{ds} = 0, V_{qs} = V_s \quad (13)$$

Thus, the components of apparent power becomes

$$P_s = -\frac{V_s M}{L_s} I_{qr} \tag{14}$$

$$Q_s = -\frac{M V_s}{L_s} I_{dr} + \frac{V_s^2}{\omega_s L_s} \tag{15}$$

Solving the equations (1) to (8), the rotor voltages in terms of rotor currents are obtained as

$$V_{dr} = R_r I_{dr} - a \rho L_r \omega_s I_{qr} + \rho L_r \frac{dI_{dr}}{dt} \tag{16}$$

$$V_{qr} = R_r I_{qr} + a \rho L_r \omega_s I_{dr} + \frac{a M V_s}{L_s} + \rho L_r \frac{dI_{qr}}{dt} \tag{17}$$

Where  $a$  is the slip and  $\rho \left( = 1 - \frac{M^2}{L_s L_r} \right)$  is dispersion coefficient.

#### 4. Identification method

Recently, the identification of dynamics based on relay experiments has received a lot of attention. It is not possible to design PID controllers or any other conventional controllers if the dynamics of the system is not known. In the literature various methods of identifying different types of systems are proposed. System identification plays a crucial role in the control of controller parameters. In relay feedback approach, the relay is connected in series with the process. The system will produce a uninterrupted oscillations, called as limit cycle. This cycle contains important process details in the form of frequency and peak amplitude (Åstrom K.J. & Hägglund T. 1984). The parameters of reduced model are therefore obtained using the information from limit cycle.

The dynamics of the DFIG system in 6<sup>th</sup> order model is suggested by (Bharti O. P. et. al. 2016)

$$G_{Actual}(s) = \frac{0.00032s^6 - 1.75s^5 - 2366s^4 + 7.9e6s^3 + 7.5e9s^2 + 5e12s + 2.18e14}{s^6 + 2340s^5 + 8.67e6s^4 + 4.79e9s^3 + 2.7e12s^2 + 1.27e14s + 9.6e14} \tag{18}$$

Relay feedback identification technique can be adopted to reduce any higher order system model to a lower order system model (Padhan D.G. & Majhi S. 2013). So, here sixth order system is modelled as the second order transfer function model

$$G_{Identified}(s) = \frac{K e^{-\phi s}}{(\tau_1 s + 1)(\tau_2 s + 1)} \tag{19}$$

The state space model of equation (19) in the Jordan Canonical form expressed as

$$\dot{q}(t) = Aq(t) + Bu(t - \phi) \tag{20}$$

$$y(t) = Cq(t) \tag{21}$$

Where

$$A = \begin{bmatrix} -\frac{1}{\tau_1} & 0 \\ 0 & -\frac{1}{\tau_2} \end{bmatrix}; B = \begin{bmatrix} 1 \\ 1 \end{bmatrix}; C = \frac{K}{\tau_1 - \tau_2} [1 \quad -1] \tag{22}$$

If a relay experiment is conducted by employing a symmetrical relay of height  $\pm \varepsilon$ , then for  $0 \leq t \leq \phi$  the limit cycle output expression is given by

$$y(t) = Ce^{At}q(0) + CA^{-1}(e^{At} - I)B\varepsilon \quad (23)$$

Suppose  $\tau$  be the half time period of one cycle of the sustained oscillations. Thus, for  $\phi \leq t \leq \tau$  the limit cycle output expression will be

$$y(t) = Ce^{A(t-\phi)}q(\phi) - CA^{-1}(e^{A(t-\phi)} - I)B\varepsilon \quad (24)$$

The sustained oscillations are obtained by considering the following constraints

$$y(0) = Cq(0) = -y(\tau) = 0 \quad (25)$$

Letting  $t = \tau$  in (24) and using of (23), the initial value gives

$$q(0) = (I + e^{A\tau})^{-1} A^{-1} (2e^{A(\tau-\phi)} - e^{A\tau} - I) B\varepsilon \quad (26)$$

The peak output  $M_p$  is obtained as

$$M_p = C \left( e^{A(\tau_p-\phi)} q(\phi) - A^{-1} (e^{A(\tau_p-\phi)} - I) B\varepsilon \right) \quad (27)$$

Where  $\tau_p$  is the time instant of positive peak.

The peak time  $\tau_p$  is obtained as

$$\tau_p = \phi + \frac{\tau_1 \tau_2}{\tau_1 - \tau_2} \ln \left( \frac{1 + e^{-\tau/\tau_1}}{1 + e^{-\tau/\tau_2}} \right) \quad (28)$$

Substituting A, B and C in (26) and (27) yield

$$\tau_1 (1 + e^{-\tau/\tau_2}) (2e^{-(\tau-\phi)/\tau_1} - e^{-\tau/\tau_1} - 1) - \tau_2 (1 + e^{-\tau/\tau_1}) (2e^{-(\tau-\phi)/\tau_2} - e^{-\tau/\tau_2} - 1) = 0 \quad (29)$$

$$M_p = k\varepsilon \left( 2(1 + e^{-\tau/\tau_1})^{\frac{-\tau_1}{\tau_1-\tau_2}} (1 + e^{-\tau/\tau_2})^{\frac{\tau_2}{\tau_1-\tau_2}} - 1 \right) \quad (30)$$

(28), (29) and (30) are simultaneously resolved to measure  $\phi$ ,  $\tau_1$  and  $\tau_2$  from the values of  $\tau$ ,  $M_p$  and  $\tau_p$ . The stable state gains  $K$  is thought to be known a priori or can be measured from a step-by-step signal test. Care has been taken to resolve the set of offline values so that the merger does not occur in a false answer.

Thus, the 6<sup>th</sup> order is identified as SOPDT given by

$$G_{Identified}(s) = \frac{0.2275e^{-0.1s}}{(0.31s + 1)(32.26s + 1)} \quad (31)$$

From Figure. 2, it is confirmed that the identified model behaves exactly same as actual DFIG model since the Nyquist plots of both cases are almost overlapping.

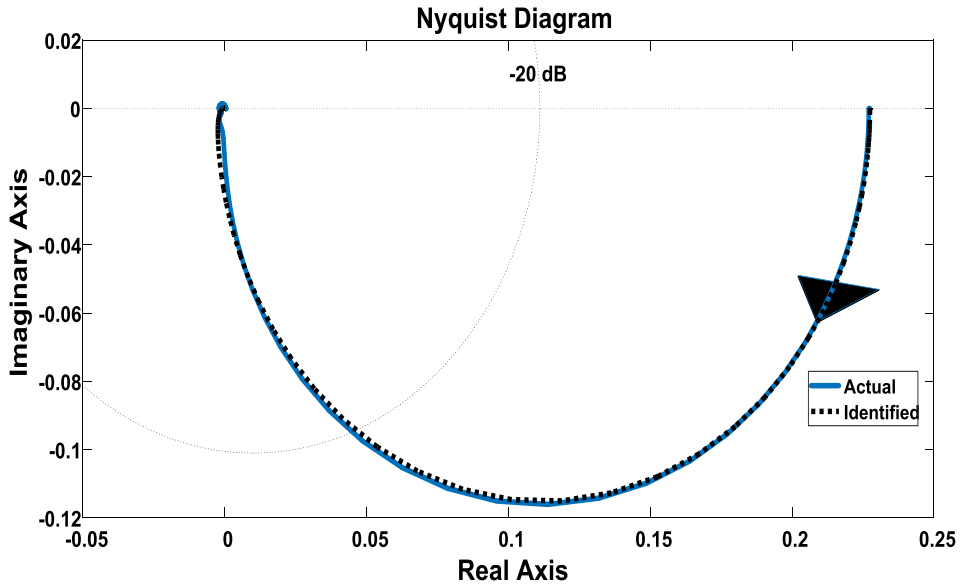


Figure. 2. Nyquist plot for Actual and identified DFIG Systems

### 5. Control Strategy and Controller Design

Mostly, the rotor current is controlled by the internal field current control loop. The shape of the field may be related to the DFIG stator flux or grid flux. From the d-q reference frames, the developed torque is determined from the q-component of the rotor current while d-component is useful in determining the reactive power at the stator terminals.

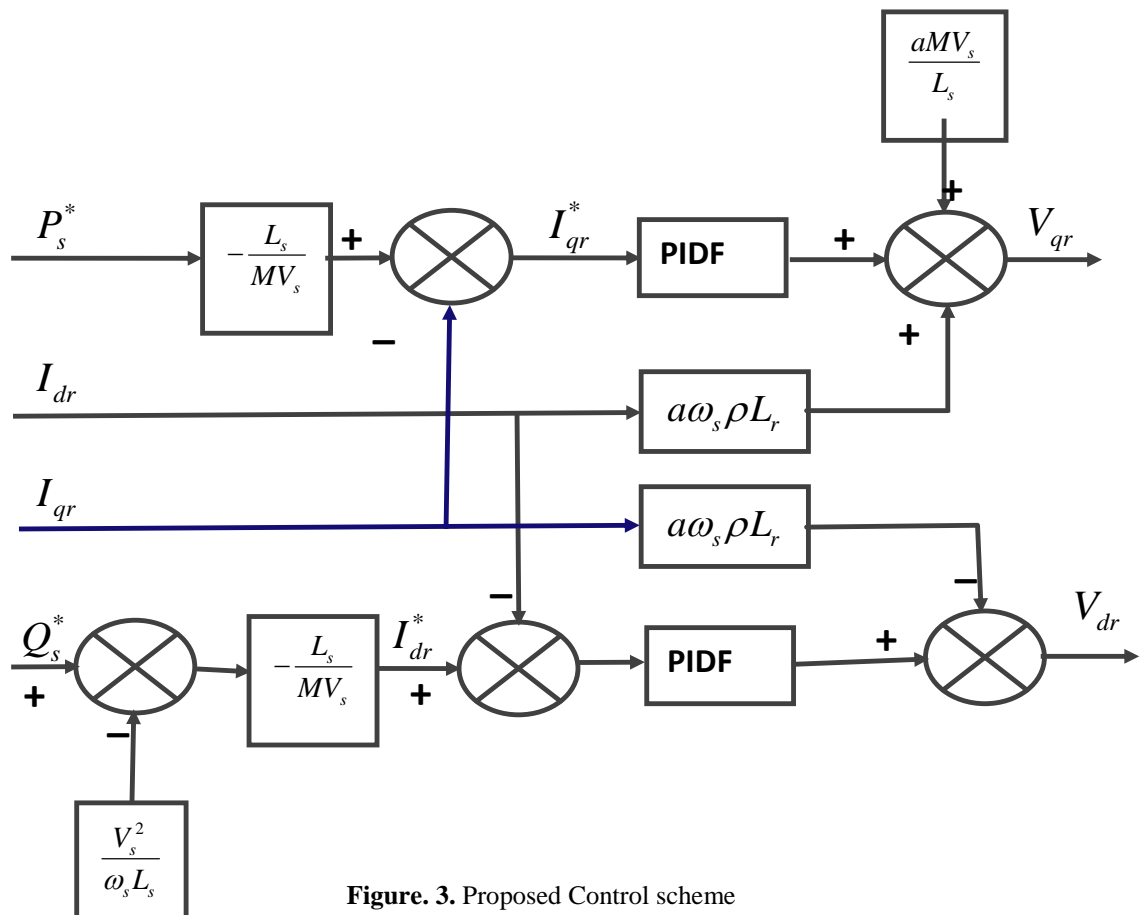
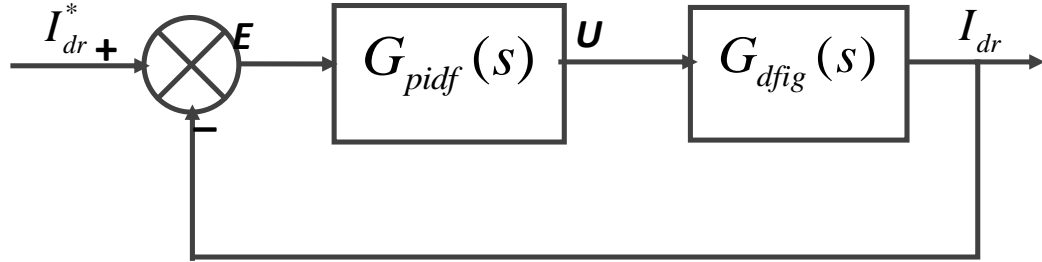


Figure. 3. Proposed Control scheme

The PIDF controller provides the ability to reject external disturbance and gives significant improved performance than PI controller. Thus, for current loop and torque control loop, the PIDF controller is recommended. One of the responsibilities of PIDF regulators is to close the gap between the perceived apparent power and the relative apparent power. In Figure. 3, as the value of the slip is weak, independent PIDF controller is employed in each current control loop to compensate the distortion successfully. In Figure. 4, the control scheme consists of two similar loops such as one loop with  $I_{dr}$  and another loop with  $I_{qr}$ .



**Figure. 4.** Block diagram representation of d-component current control loop with PIDF controller

The PIDF control structure is considered as

$$G_{pidf}(s) = K_c \left( 1 + \frac{1}{T_i s} + T_d s \right) \times \frac{1}{\tau_c s + 1} \quad (32)$$

The parameters  $K_c$ ,  $T_i$  and  $T_d$  are obtained using direct synthesis approach (Seshagiri Rao A. et al. 2009).  $\tau_c$  is the tuning parameter of first order filter and selected to achieve satisfactory closed loop response.

The closed-loop transfer function for the current loop is

$$\frac{I_{dr}}{I_{dr}^*} = \frac{G_{pidf}(s)G_{dfig}(s)}{1 + G_{pidf}(s)G_{dfig}(s)} \quad (33)$$

Using direct synthesis method, the desired closed loop response is specified and the corresponding PIDF controller is obtained.

Hence equation (33) gives

$$G_{pidf}(s) = \frac{1}{G_{dfig}(s)} \frac{1}{\left( \frac{I_{dr}}{I_{dr}^*} \right)_{desired} - 1} \quad (34)$$

Choosing the desired closed loop dynamics as

$$\left( \frac{I_{dr}}{I_{dr}^*} \right)_{desired} = \frac{e^{-\phi s}}{\beta_c s + 1} \quad (35)$$

Where  $\phi$  is the time delay of the desired system and  $\beta_c$  is the closed loop tuning parameter. Thus,

$$G_{pidf}(s) = \frac{(\tau_1 s + 1)(\tau_2 s + 1)}{K(\beta_c s + 1 - e^{-\phi s})} \quad (36)$$

From (34) and (36), the following controller parameters were obtained by setting  $\beta_c = \phi$ .

$$\left. \begin{aligned} K_c &= \frac{0.5(\tau_1 + \tau_2)}{K\phi} \\ T_i &= \tau_1 + \tau_2 \\ T_d &= \frac{\tau_1\tau_2}{\tau_1 + \tau_2} \end{aligned} \right\} \quad (37)$$

## 6. Selection of filter tuning parameter $\tau_c$

The main prerequisite for the choice of  $\tau_c$  is that the benefits of the emerging controller should have good K values. In addition, the led controller should be selected in such a way as to provide better performance in case of perfect model and system parameter perturbation cases. After extensive simulation, it was found that the initial value of the  $\tau_c$  can be assumed to be equal to a quarter of the process delay. If a satisfactory result is not obtained by this number, then the configuration parameter can gradually increase from this value to the optimal performance of nominal and robust responses. By comparison, the value of the adjustment parameter that provides optimal control performance is selected between the range  $0.25\phi - 2\phi$ .

## 7. Performance measure

### 7.1. Integral Error Criteria

Three well-known performance indicators are used to assess performance based on integral error: ITAE, IAE and ISE (Sigurd Skogestad 2003). Error signal is the difference between desired output and actual output. Thus, integral errors are given by

$$ITAE = \int_0^{\infty} t |e(t)| dt \quad (38)$$

$$IAE = \int_0^{\infty} |e(t)| dt \quad (39)$$

and

$$ISE = \int_0^{\infty} (e(t))^2 dt \quad (40)$$

The ISE standard punishes large errors, while the ITAE standard punishes long-term errors. The IAE standard generates controller settings between the ITAE and ISE standards.

### 7.2. Total Variation (TV)

To estimate the control effort, basically TV of the input  $u(t)$  has to be calculated. Generally, TV is the sum of all its movements up and down (Sigurd Skogestad 2003). Mathematically,

$$TV = \sum_{i=1}^{\infty} |u_{i+1} - u_i| \quad (41)$$

The overall difference should be as small as possible. TV is a nice measure of the sleekness of control variable.

## 8.Simulation results

Consider the dynamics of DFIG system is obtained by (Bharti O. P. et. al. 2017)

$$G_{Actual}(s) = \frac{0.00032s^6 - 1.75s^5 - 2366s^4 + 7.9e6s^3 + 7.5e9s^2 + 5e12s + 2.18e14}{s^6 + 2340s^5 + 8.67e6s^4 + 4.79e9s^3 + 2.7e12s^2 + 1.27e14s + 9.6e14}$$

The corresponding SOPDT model of DFIG system is

$$G_{Identified}(s) = \frac{Ke^{-\theta s}}{(\tau_1 s + 1)(\tau_2 s + 1)} = \frac{0.2275e^{-0.1s}}{(0.31s + 1)(32.26s + 1)}$$

Using the proposed method, parameters of controller PIDF is obtained as:  $K_c = 714.28$ ,  $T_i = 32.5$ ,  $T_d = 0.307$ , and  $\tau_c = 0.1$ . For simulation studies, at  $t=10$  sec a desired step signal of magnitude 1 pu is enforced. A negative step load input is applied at  $t=200$  sec. Figure. 5 shows the current loop responses for perfect model and the corresponding control variables are demonstrated in Figure. 6. To display the improvement of the proposed method, (Bharti O. P. et al. 2016) technique is considered here. The controller settings  $K_p = 39.9781$ ,  $K_i = 7.6902$  and  $K_d = 0.0271$  are suggested by Bharti et al PSO-PID. The PID controllers parameters  $K_p = 0.1417$ ,  $K_i = 0.1472$  and  $K_d = 0.1005$  are proposed by Bharti et al for BFA-PID. From Figure.5 and Figure. 6, It is clear that the proposed approach provides better servo and regulatory performance than Bharti et al.

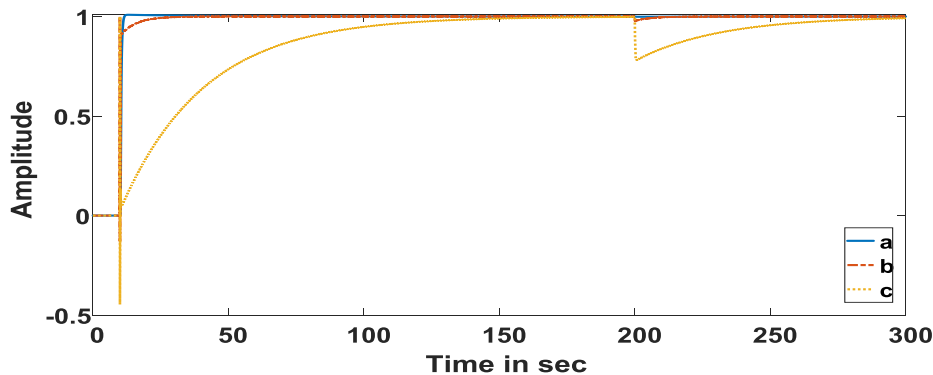


**Figure. 5:** Set-point current response and External Disturbance rejection response for nominal case: a-proposed, b-Bharti PSO PID, c-Bharti BFA PID

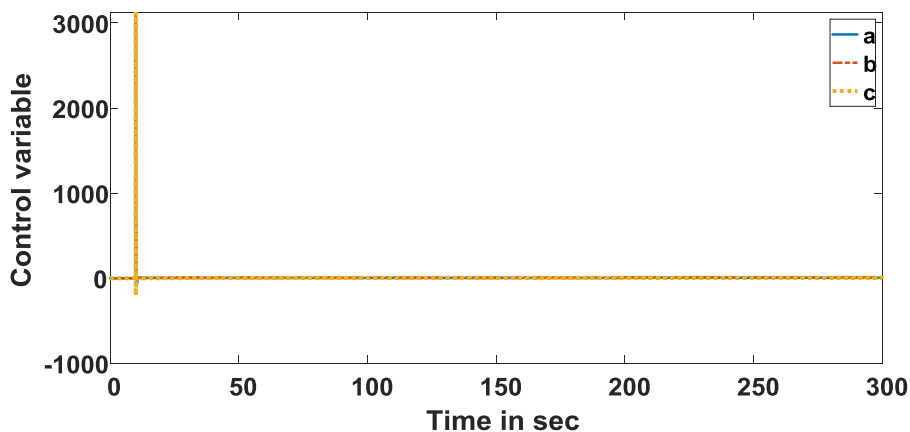


**Figure. 6:** Manipulated current controller response for nominal case: a-proposed, b-Bharti PSO PID, c-Bharti BFA PID

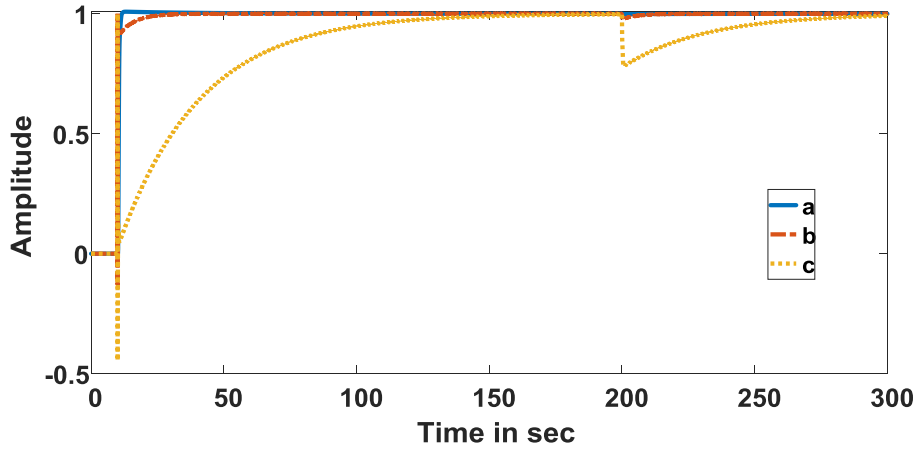


**Figure. 7:** Current responses for perturbations for +25% deviation in stator and rotor parameters: a-proposed, b-Bharti PSO PID, c-Bharti BFA PID

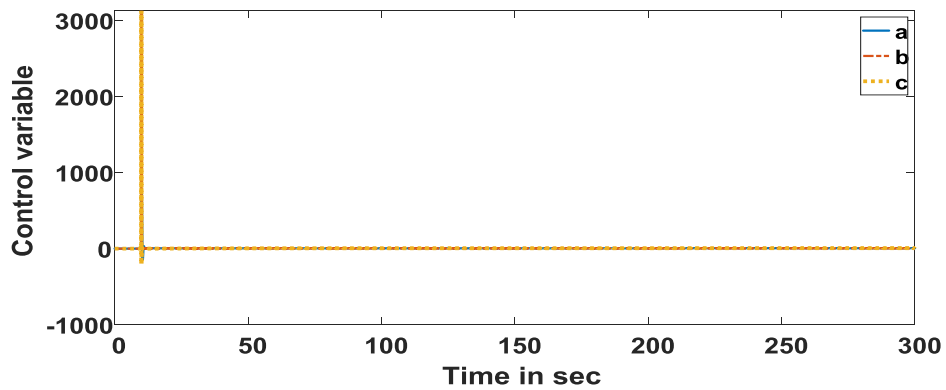


**Figure. 8:** Manipulated perturbed responses for +25% deviation in stator and rotor parameters: a-proposed, b-Bharti PSO PID, c-Bharti BFA PID

In order to check the robustness of PIDF, the stator and rotor parameters are changed by +25%. The outputs of current loop and the corresponding controller outputs are shown in Figure. 7 and Figure. 8. Clearly, the proposed method gives improved closed loop performances. For more clarity, the current servo responses and regulatory responses are analysed separately.

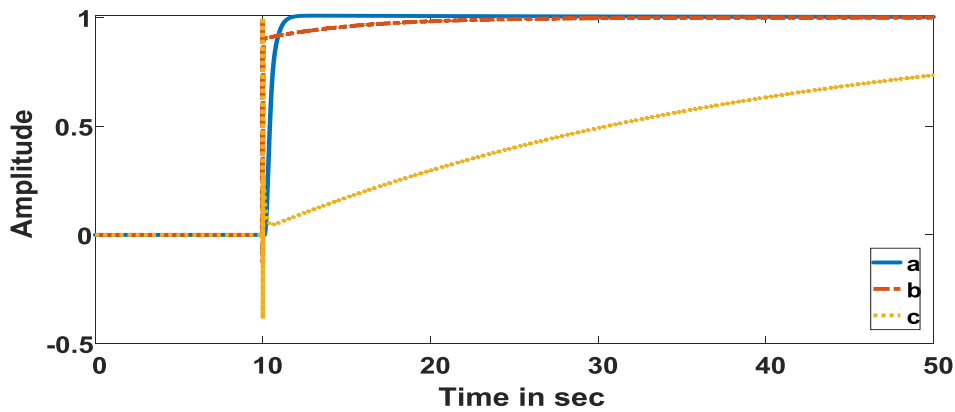


**Figure. 9** Set-point current response for nominal case: a-proposed, b-Bharti PSO PID, c-Bharti BFA PID

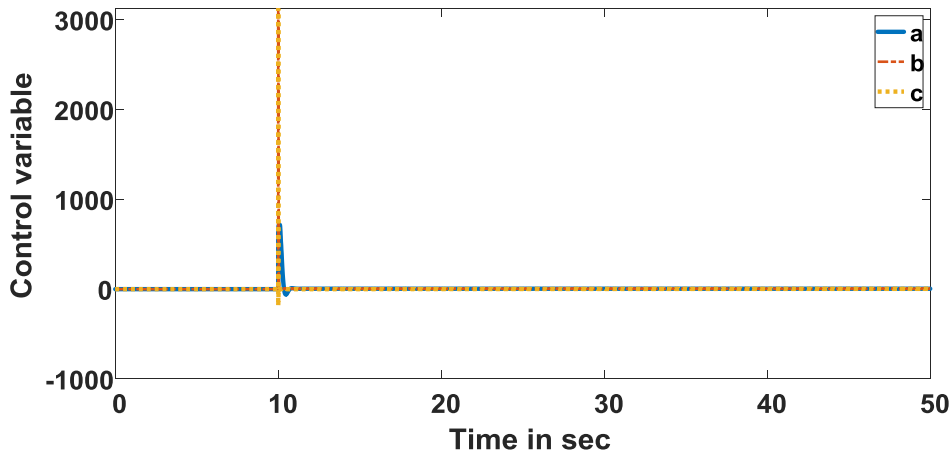


Figure. 10 Set point current control variable nominal case: a-proposed,b- Bharti PSO PID, c-Bharti BFA PID

An input step signal with amplitude 1 pu is used at  $t = 10$  sec. The Figure. 9 and Figure. 10 show the nominal current tracking responses and the corresponding control variables, respectively. It is noticed that better set point responses with less variation in the control output are achieved with proposed PIDF controller.

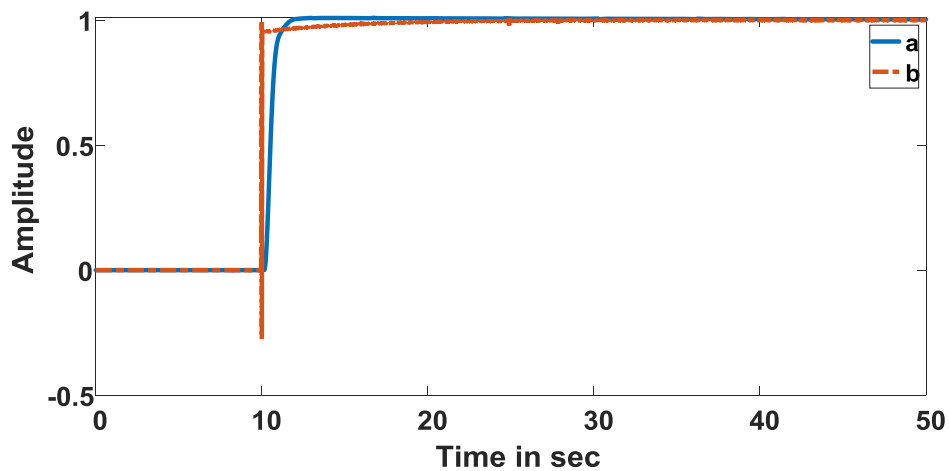


Figure. 11: Set-point current for perturbation of +50% in rotor and stator parameters: a-proposed, b-Bharti PSO PID

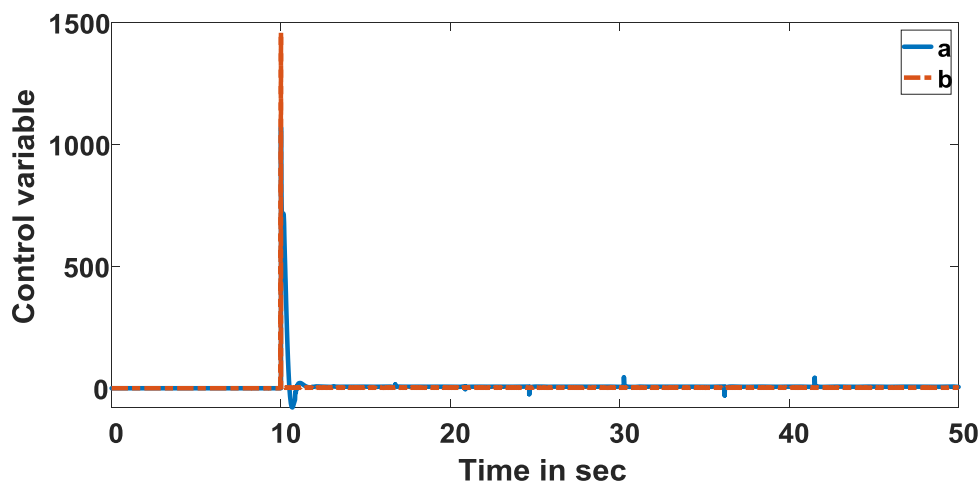
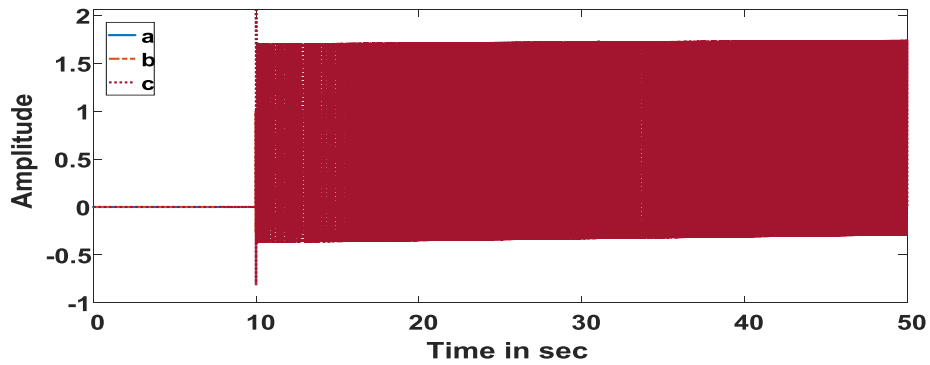
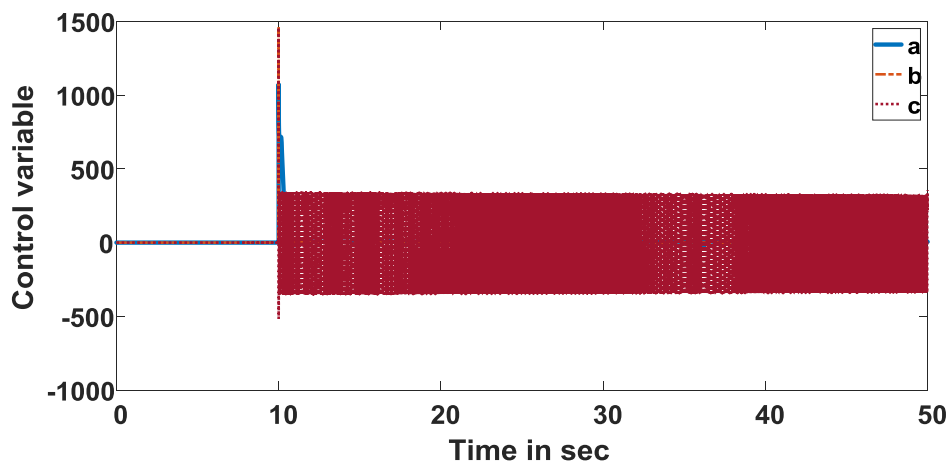


Figure. 12: Manipulated current for perturbation of +50% in rotor and stator parameters: a-proposed, b-Bharti PSO PID



**Figure. 13:** Set-point current for +50% variation in stator and rotor parameters: a-proposed, b-Bharti PSO PID, c-Bharti BFA PID



**Figure. 14:** Manipulated current for perturbation of +50% in rotor and stator parameters: a-proposed, b-Bharti PSO PID, c-Bharti BFA PID

Now, the stator and rotor parameters are changed by +50% for analysing the worst case scenarios. The set point responses and control variables are shown in Figure.11, Figure. 12, Figure. 13 and Figure.14. From Figure. 11 and Figure. 12, it is noticed that proposed PIDF controller gives satisfactory closed loop responses with zero overshoot. Even Bharti PSO PID controller has overshoot in the servo response with the expense of more control action. Figure. 11 and Figure. 12 do not show the responses of Bharti BFA PID as these responses are highly oscillatory. For clarity, the simulation results of these oscillatory responses are shown in Figure. 13 and Figure. 14.

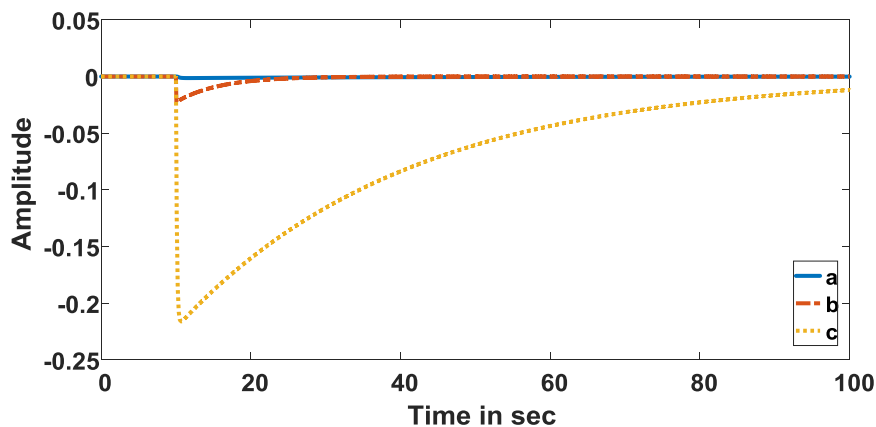


**Figure. 15:** External Disturbance rejection responses for nominal case: a-proposed, b-Bharti PSO PID, c-Bharti

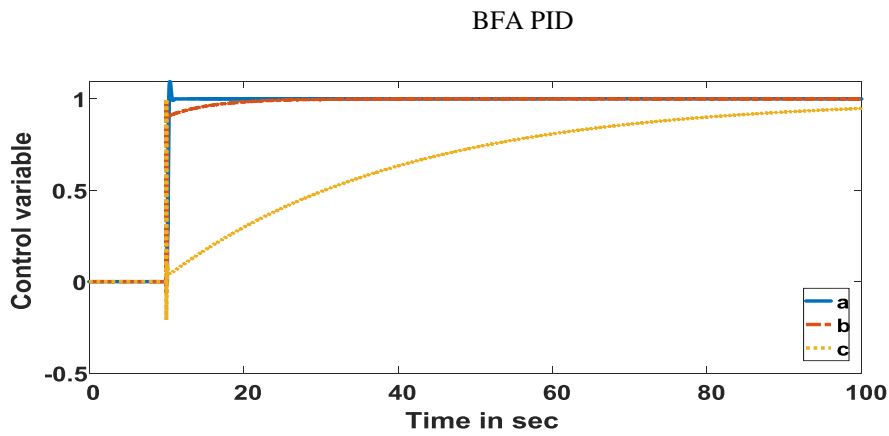


**Figure. 16:** Manipulated current controller response for external disturbance in nominal case: a-proposed, b-Bharti PSO PID, c-Bharti BFA PID

With all these controller parameters, the performance of the closed loop control system is tested by applying a negative step in load at  $t = 10$  sec. Figure. 15 and Figure. 16 shows answer if there are no similarities in the process and model. It can be seen that the methods of Bharti et al provided a slow control effect. The proposed approach provides a better response to the disruption. However, it ought to be noted that in apply there are continuously differences within the model of plants. Therefore, control performance ought to even be assessed considering that there is uncertainty in the DFIGmodel.

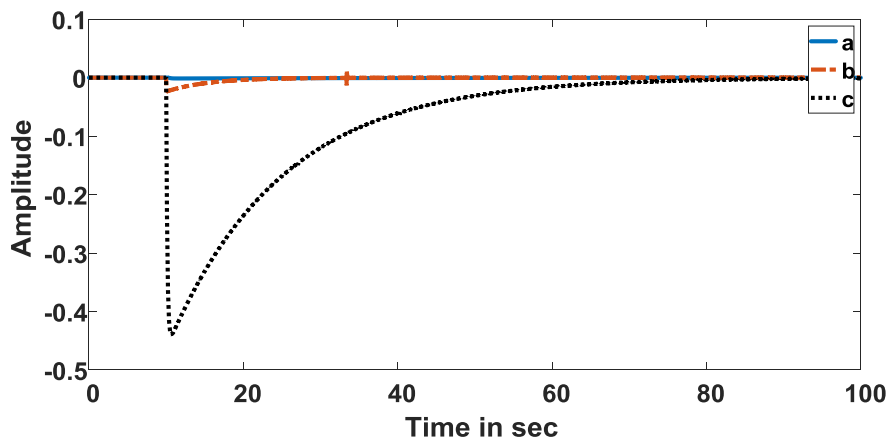


**Figure. 17:** External disturbance rejection responses for +50% variation in stator and rotor parameters: a-proposed, b-Bharti PSO PID, c-Bharti BFA PID

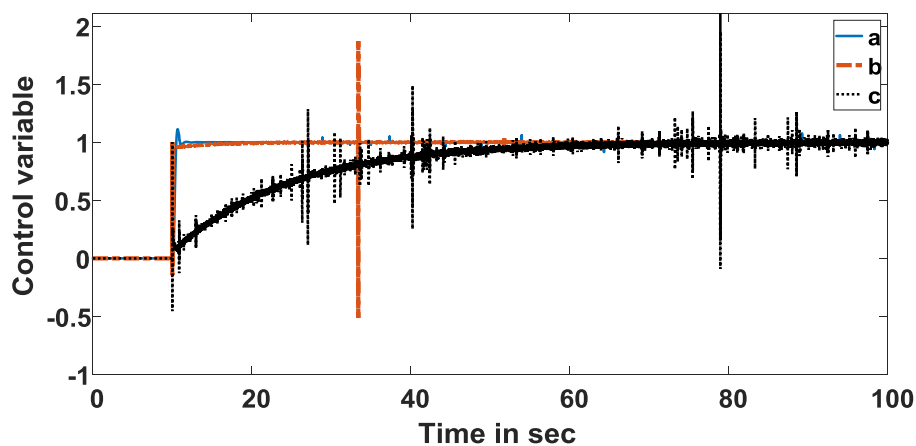


**Figure. 18:** Manipulated current controller response for disturbance rejection in +50% variation in stator and rotor parameters: a- proposed, b-Bharti PSO PID, c-Bharti BFA PID

In the current operation, it is considered + 50% distortion of the stator and rotor parameters. Disturbed responses and variability of the corresponding controls are shown in Figure. 17 and Figure. 18 respectively. It can be seen that the proposed method provides better control performance.

**Table 1.** Performance Specifications of setpoint responses

	Nominal Case			Perturbed Case		
	ITAE	IAE	ISE	ITAE	IAE	ISE
Proposed	10.49	0.6874	0.347	11.43	0.772	0.43
Bharti et al PSO PID	8.951	0.5723	0.334	4.13	0.267	0.008
Bharti et al BFA PID	561.6	21.76	13.44	908.2	30.44	29.96

**Table 2.** Performance Specifications of disturbance rejection responses

	Nominal Case			Perturbed Case		
	ITAE	IAE	ISE	ITAE	IAE	ISE
Proposed	1.569	0.0427	$3.173 \times 10^{-5}$	1.576	0.042	$3.167 \times 10^{-5}$
Bharti et al PSO PID	2.054	0.1301	0.0014	2.028	0.13	0.0015
Bharti et al BFA PID	229.9	6.428	0.7452	167.6	6.77	1.546

**Table 3.** Performance Specifications of Control Signals for set point responses

	Nominal Case	Perturbed Case
	TV	TV
Proposed	$1.8135 \times 10^3$	$2.7242 \times 10^3$
Bharti et al PSO PID	$7.0421 \times 10^3$	$4.5433 \times 10^3$
Bharti et al BFA PID	$1.4815 \times 10^4$	$2.9363 \times 10^7$

**Table 4.** Performance Specifications of Control Signals for disturbance rejection responses

	Nominal Case	Perturbed Case
	TV	TV
Proposed	2.2977	3.0169
Bharti et al PSO PID	32.6105	116.0449
Bharti et al BFA PID	119.6202	$3.0513 \times 10^3$

To compare all the methods quantitatively, the ITAE, IAE and ISE performance criteria are considered in this paper. Table 1 shows the performance criteria for servo responses. The various interference input errors are recorded in Table 2. Thus, from Table 1 and Table 2, it is confirmed that the proposed method gives lower error values. A complete variation of the control efforts is given in Table 3 and Table 4. It is observed that the proposed TV is low compared to other alternatives. Therefore, the designed method provides a smooth control effort. Obviously, the proposed method works better.

### 9. Robustness Analysis

Kharitonov Theorem has been used to check the robustness of DFIG control system. Kharitonov Theorem says that an interval polynomial family with invariant degree is stable if and only if its four Kharitonov polynomials are stable (**Padhan D.G. & Majhi S. 2013**). The development of Kharitonov polynomials relies on special fastened sequence of upper and lower bounds of coefficients in interval polynomial (**Ravikumar N. V. A. & Saraswathi G. 2019**).

Given the interval polynomial as

$$p(s, q) = q_0 + q_1s + q_2s^2 + q_3s^3 + \dots + q_n s^n \quad (42)$$

$$p(s, q) = (q_0^{lo} \ q_0^{hi}) + (q_1^{lo} \ q_1^{hi})s + (q_2^{lo} \ q_2^{hi})s^2 + \dots + (q_n^{lo} \ q_n^{hi})s^n \quad (43)$$

where  $(q_i^{lo} \ q_i^{hi})$  represents the bounding interval for the  $i^{th}$  component of uncertainty  $q_i$ . An polyniial family with invariant degree is robustly stable if and given that the subsequent four Kharitonov polynomials are strictly stable.

$$\left. \begin{aligned} K_1(s) &= q_0^{lo} + q_1^{lo} s + q_2^{hi} s^2 + q_3^{hi} s^3 + q_4^{lo} s^4 + \dots \\ K_2(s) &= q_0^{hi} + q_1^{hi} s + q_2^{lo} s^2 + q_3^{lo} s^3 + q_4^{hi} s^4 + \dots \\ K_3(s) &= q_0^{hi} + q_1^{lo} s + q_2^{lo} s^2 + q_3^{hi} s^3 + q_4^{hi} s^4 + \dots \\ K_4(s) &= q_0^{lo} + q_1^{hi} s + q_2^{hi} s^2 + q_3^{lo} s^3 + q_4^{lo} s^4 + \dots \end{aligned} \right\} \quad (44)$$

The denominator polynomials of the current loop transfer function given by

$$1 + G_{pidf}(s)G_{dfig}(s) = 0 \quad (45)$$

$$G_{dfig}(s) = \frac{Ke^{-\phi s}}{(\tau_1 s + 1)(\tau_2 s + 1)} = \frac{0.2275e^{-0.1s}}{(0.31s + 1)(32.26s + 1)}$$

The time delay term  $e^{-\phi s}$  is approximated as  $R_{3,4}$  Pade approximation [23] given by

$$e^{-\phi s} = \frac{840 - 360s\phi + 60(s\phi)^2 - (s\phi)^3}{840 + 480s\phi + 120(s\phi)^2 + 16(s\phi)^3 + (s\phi)^4}$$

$$G_{pidf}(s) = K_c \left( 1 + \frac{1}{T_i s} + T_d s \right) \times \frac{1}{\tau_c s + 1} = 714.28 \left( 1 + \frac{1}{32.5s} + 0.307s \right) \times \frac{1}{0.1s + 1}$$

The interval polynomials of DFIG system is obtained as

$$\begin{aligned} p(s, q) &= [3359.328 \ 5038.992] + [109727.1552 \ 164590.7328]s + [50724.3633 \ 76086.545]s^2 \\ &+ [6610.2328 \ 9915.3493]s^3 + [439.0281 \ 658.5422]s^4 + [9.9762 \ 14.9643]s^5 \\ &+ [0.1306 \ 0.1959]s^6 + [0.0008 \ 0.0012]s^7 \end{aligned}$$

Now, the four Kharitonov polynomials are

$$\begin{aligned} K_1(s) &= 3359.328 + 109727.1552s + 76086.545s^2 + 9915.3493s^3 + 439.0281s^4 + 9.9762s^5 + 0.1959s^6 + 0.0012s^7 \\ K_2(s) &= 5038.992 + 164590.7328s + 50724.3633s^2 + 6610.2328s^3 + 658.5422s^4 + 14.9643s^5 + 0.1306s^6 + 0.0008s^7 \\ K_3(s) &= 5038.992 + 109727.1552s + 50724.3633s^2 + 9915.3493s^3 + 658.5422s^4 + 9.9762s^5 + 0.1306s^6 + 0.0012s^7 \\ K_4(s) &= 3359.328 + 164590.7328s + 76086.545s^2 + 6610.2328s^3 + 439.0281s^4 + 14.9643s^5 + 0.1959s^6 + 0.0008s^7 \end{aligned}$$

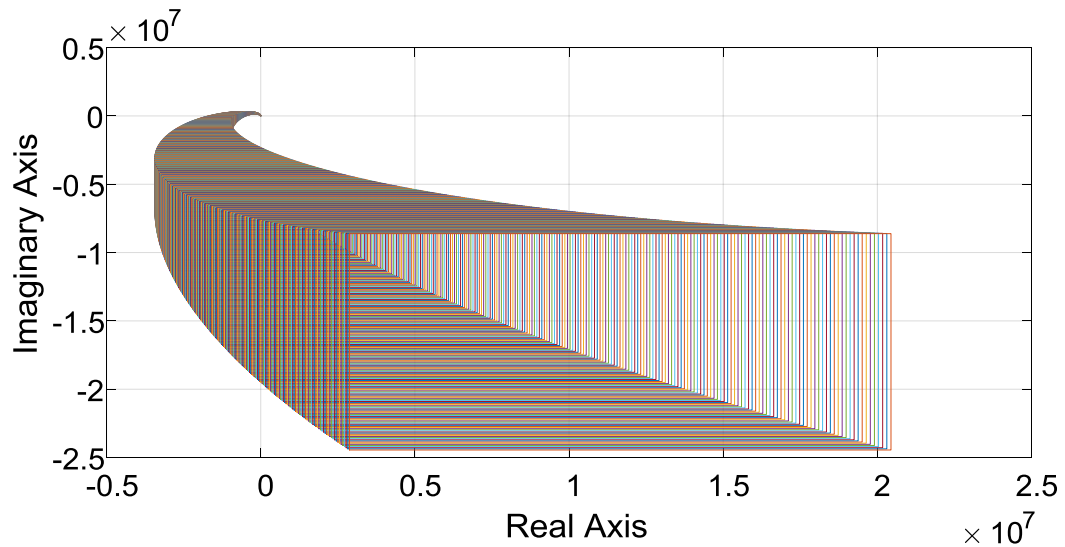


**Figure. 19** Kharitonov rectangles – Zero Exclusion Condition

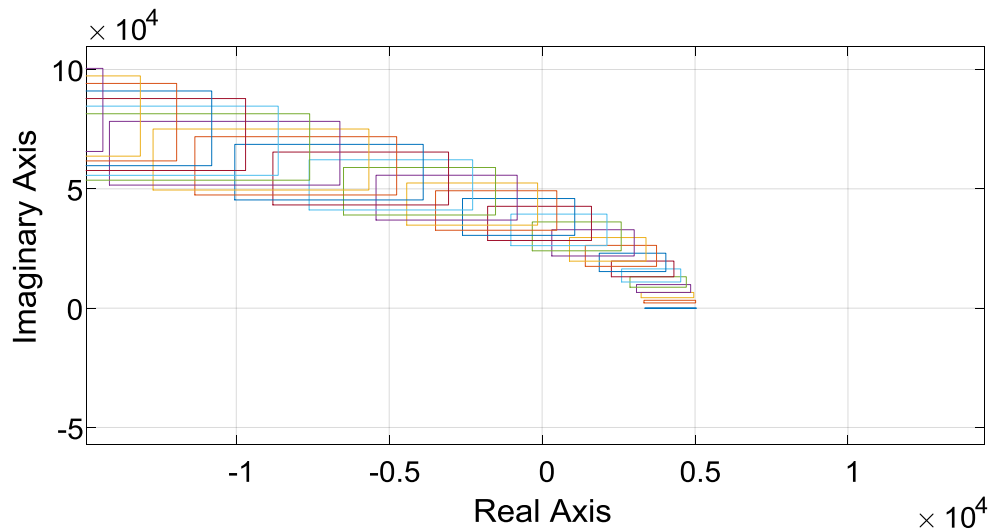


**Figure. 20:** Zoomed Kharitonov rectangle of Figure 19

In order to determine robustness, 20% uncertainty was observed in crop boundaries. The Kharitonov rectangles of the control system are shown in Fig. 19. From Fig. 19, it's clear that the Kharitonov rectangles are moving in the background with anti-clockwise so that the monotonic class can expand the properties of Hurwitz polynomials. The graph is zoomed (see Figure. 20) to point out the state of the output at zero. It's evident that the control system measure of the system is stable in a complex plane in Mikhailov's concept. As the origin is excluded from the Kharitonov rectangle (Figure 19) it's clear that the control of the DFIG system is firmly established. The main advantage of the designed technique is that it's easy with a typical structure and therefore simple for the operator. The proposed method provides simple tuning expression for the PIDF controller and provides the exact value. Previous methods do not provide specific values for the control parameters. Within the planned technique, there are two parameters to be chosen, namely the specified closed-loop system time constant and first order filter time constant. The calibration parameter, i.e. desired closed loop system time constant to be considered as  $\phi$ . Also, it has already been shown by simulation that the first order filter tuning parameter can be considered  $0.25\phi - 2\phi$ . Guidelines are also provided for the choice of this configuration parameter therefore the designed technique is easy to use online and easy to configure.

## 8. Conclusion

The higher order dynamics of DFIG system is reduced to a second order and dead time model by conducting a relay experiment. An easy controller design methodology is suggested for a variable speed DFIG-based WECS using direct synthesis approach, to prevent system breakdown under extreme conditions. Guidelines are provided for the choice of the tuning parameters. The nominal and robust control performances are enhanced with the designed controller. Significant improvements are being made in comparison to the methods recently reported in open literature. Simulation results show that WECS with PIDF controls show better performance even in critical situations. This is reflected in the robustness to rotor resistance variation and superior disturbance-rejection. Using the Kharitonov theorem, and therefore the zero-exclusion condition, robustness is clearly examined diagrammatically. The DFIG system is extremely versatile in terms of design and variability of stator and rotor parameters.

## References

1. Ravichandran S., Kumudinidevi R. P., Bharathidasan S. G., and Evangelin Jeba V. (2014). Coordinated controller design of grid connected DFIG based wind turbine using response surface methodology and NSGAI, *Sustain. Energy Technol. Assessments*, 8, 120–130.
2. Tripathi P. M., Sahoo S. S, Chatterjee K. (2018). Enhancement of low-voltage ride through of wind energy conversion system using superconducting saturated core fault current limiter, *Int. Trans. Electr. Energy Syst.*, 2, 2798.
3. Kumar R., Agrawal H.P., Shah A, Bansal H.O. (2019). Maximum power point tracking in wind energy conversion system using radial basis function based neural network control strategy, *Sustain. Energy Technol. Assessments*, 36, 1–10.
4. Mebrahtu F., Khan B., Haes H. (2020). Analyzing low voltage ride through capability of doubly fed induction generator based wind turbine, *Computers & Electrical Engineering*, 86, 106727.
5. Singh Bhim, Shiv Kumar Aggarwal, Tara Chandra Kandpal (2010). Performance of Wind Energy Conversion System Using a Doubly Fed Induction Generator for Maximum Power Point Tracking, *IEEE Industry Applications Society Annual Meeting*, 139(5), 429-442.
6. Huabin Wen, Yu Zeng, Lei Wang, Feng Yang, Song Y. D. (2014). Robust Adaptive Reactive Power Control for Doubly Fed Induction Generator, *Abstract and Applied Analysis*, 14, 1-8.
7. Taveiros F.E.V, Barros L.S., Costa F.B. (2015). Back-to-back converter state-feedback control of DFIG (doubly-fed induction generator)-based wind turbines, *Energy*, 89, 896-906.
8. Pena R., Clare J.C., Asher G. M. (1996). Doubly fed induction generator using back-to-back PWM converters and its application to variable-speed wind-energy generation, *IEE Proc. – Electr. Power Appl.*, 143(3), 3-17.
9. Åstrom KJ, Hägglund T (1984). Automatic tuning of simple regulators with specifications on phase and amplitude margins, *Automatica*, 20(5), 645–5.
10. Padhan DG, Majhi S (2013). A new control scheme for PID load frequency controller of single-area and multi-area power systems, *ISA Transactions*, 52(2), 242–51.
11. Tremblay E., Atayde S., Chandra A. (2011). Comparative Study of Control Strategies for The Doubly Fed Induction Generator in Wind Energy Conversion Systems: A DSP-Based

- Implementation approach, IEEE Trans. Sustain. Energy, 2(3), 288–299.
23. Ma K., Tutelea L., Boldea I., Ionel D. M., Blaabjerg F. (2015). Power Electronic Drives, Controls, And Electric
  24. Generators For Large Wind Turbines-An Overview, Electr. Power Components Syst., 43(12), 1406–1421.
  25. Swain S., Ray P.K. (2017). Short circuit fault analysis in a grid connected DFIG based wind energy system with
  26. active crowbar protection circuit for ride through capability and power quality improvement, Int. J. Electr. Power Energy Syst., 84, 64–75.
  27. Mishra A., Tripathi P. M., Chatterjee K. (2018). A review of harmonic elimination techniques in grid connected
  28. doubly fed induction generator based wind energy system, Renew. Sustain. Energy Rev., 89.
  29. Bharti O. P., Saket R. K., Nagar S. K. (2016). Controller Design for DFIG Driven by Variable Speed Wind
  30. Turbine Using Static Output Feedback Technique, Engineering, Technology & Applied Science Research, 6(4), 1056-1061.
  31. Swami Naidu N. K., Singh B. (2016). Experimental Implementation of a Doubly Fed Induction Generator
  32. Used for Voltage Regulation at a Remote Location, IEEE Transactions on Industry Applications, 52(6), 5065-5072.
  33. Kraus F., Mansour M., Jury E. I. (1992). Robust Schur Stability of Interval Polynomials, IEEE Transactions on
  34. Automatic Control, 37(1), 141-143.
  35. Matuš R., Prokop R. (2012). Graphical Analysis of Robust Stability for Polynomials with Uncertain Coefficients
  36. in Matlab Environment, in: Proceeding of the 16th WSEAS International Conference on Systems, Kos, Greece.
  37. Seshagiri Rao A., Rao V.S.R., Chidambaram M. (2009). Direct synthesis-based controller design for integrating
  38. processes with time delay, Journal of the Franklin Institute, 346, 38–56.
  39. Sigurd Skogestad (2003). Simple analytic rules for model reduction and PID controller tuning”, Journal of Process
  40. Control, 13, 291–309.
  41. Bharti O. P., Saket R. K., Nagar S. K. (2017). Controller Design of DFIG Based Wind Turbine by Using
  42. Evolutionary Soft Computational Techniques, Engineering, Technology & Applied Science Research, 7(3), 1732-1736.
  43. Ravikumar N. V. A., Saraswathi G. (2019). Robust Controller Design for Speed Regulation of a Wind Turbine
  44. using 16-Plant Theorem Approach, EAI Endorsed Transactions on Energy Web, 6(24).
  45. Vajta M. (2000). Some Remarks On Padé-Approximations, 3rd TEMPUS-INTCOM Symposium, September 9-14.